π^0 Production and Angular Distribution Analysis: Target Material, Thickness, and Emission Angle Dependence

Baki Berkay Altunkaynak, Ceren Akgün, Fuat Berkin Altunkaynak, Mahir Kocakaya, Muhammed Yılmaz, Salih Efe Çabuk, Yusuf Tarikci

"The most beautiful thing we can experience is the mysterious. It is the source of all true art and science."

— *Albert Einstein*

Contents

1 Introduction

The neutral pion (π^0) is among the most abundantly produced particles in hadronic interactions. Because it decays almost entirely into two photons [1], it provides a clean and well-defined signature that makes it a powerful probe of the dynamics of proton–nucleus collisions. Understanding how many pions are produced, at what energies, and in which directions is essential for modelling hadronic showers in detector systems, estimating radiation environments around accelerators, and benchmarking the simulation codes that underpin modern particle physics experiments.

Pion production in nuclear targets is known to grow with the nuclear mass number [2], but the picture becomes considerably more complex in thick targets, where pions can rescatter or be reabsorbed before escaping. Previous experiments have explored related aspects of this problem: pion spectra in proton–carbon collisions at high beam momenta [3], neutral pion production in collider and neutrino-beam environments [4, 5], and angular distributions in low-energy proton–nucleus reactions [6], but none has mapped the combined effect of target material, target thickness, and emission angle in a proton–nucleus setup in the intermediate energy regime around 1 GeV/c. Our experiment is designed to fill precisely that gap.

2 Overview of the Experiment

The experiment will be carried out at the T9 beamline of the CERN PS East Area [7]. A 1 GeV/c proton beam is selected from the mixed secondary beam using two upstream Cherenkov detectors.

We study three target materials (Iron (Fe), Copper (Cu), and Tungsten (W)), each machined to four different thicknesses, giving twelve target configurations in total (Table 1). The depths span 6–70% of the nuclear interaction lengths of the materials λ_I (Fe 16.77 cm, Cu 15.32 cm, W 9.946 cm) [8], covering the transition from free pion escape to a regime where re-interactions become significant.

Setup n	Material	Diameter	Depth
1	Iron (Fe)	15 cm	1 cm
2	Iron (Fe)	15 cm	3 cm
3	Iron (Fe)	15 cm	5 cm
4	Iron (Fe)	15 cm	7 cm
5	Copper (Cu)	15 cm	1 cm
6	Copper (Cu)	15 cm	3 cm
7	Copper (Cu)	15 cm	5 cm
8	Copper (Cu)	15 cm	7 cm
9	Tungsten (W)	15 cm	1 cm
10	Tungsten (W)	15 cm	3 cm
11	Tungsten (W)	15 cm	5 cm
12	Tungsten (W)	15 cm	7 cm

Table 1: Target properties for all 12 experimental configurations.

Photons from $\pi^0 \to \gamma\gamma$ decays are detected by seven Lead-Glass calorimeters arranged $\sim$18.66 cm downstream of the target [7], covering angles between 0° and 90°. This angular

range is chosen to capture both the dominant forward signal and the large-angle tail, where predictions from different hadronic interaction models tend to disagree most [3, 6]. Each calorimeter is equipped with a veto scintillator to reject charged particles, and accidental coincidences are removed by subtracting off-time background windows [7].

The π^0 is identified through its two-photon decay: when two calorimeters register simultaneous energy deposits, the invariant mass of the photon pair is computed from their energies and opening angle. A clear peak at the known pion mass serves both as the signal and as an in-situ calibration check [1]. The experimental layout is shown in Figure 1.

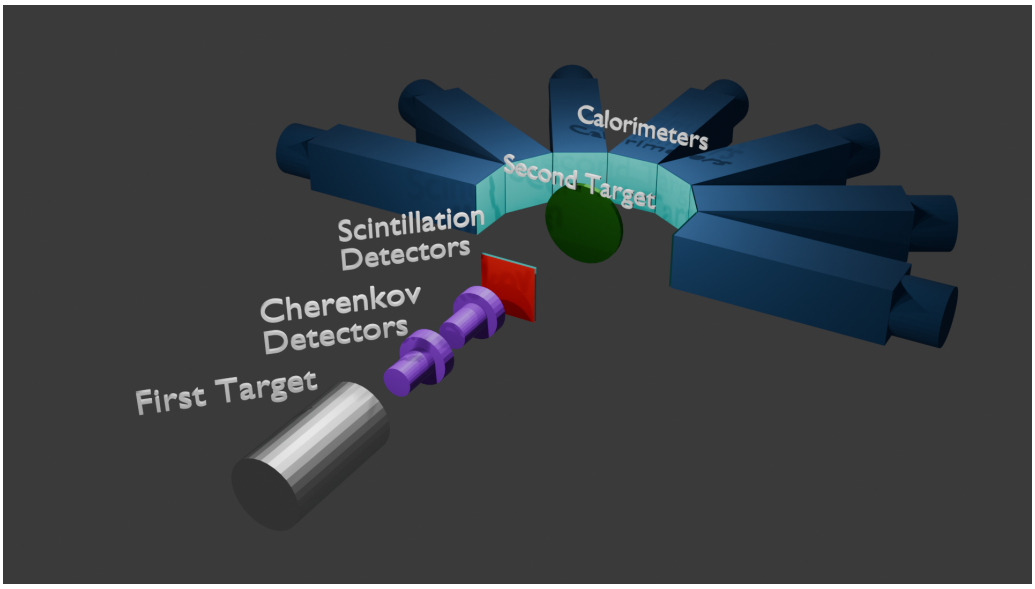

Figure 1: Schematic overview of the experimental setup.

3 Physics Goals

This experiment pursues three interconnected physics goals. Iron, Copper, and Tungsten ($A = 56$, 63, and 184 respectively) [8] span a wide range in nuclear mass number and are standard targets available at T9.

First, we measure the A^α scaling exponent by comparing yields across the three targets under identical beam conditions; a deviation would signal non-trivial nuclear effects beyond geometric scaling [6]. Second, we map the transition from linear yield growth to saturation as a function of target depth, identifying the depth at which secondary interactions begin to suppress net π^0 output [2, 6]. Third, we measure the π^0 angular distribution and test whether it broadens with increasing nuclear mass, as expected from multiple scattering and transverse momentum enhancement in heavier nuclei [9]. The range 0°–90° covers the dominant forward signal and the large-angle tail where hadronic models disagree most strongly [3, 6], providing the most sensitive test of the underlying interaction dynamics.

All yields are compared against Geant4 [10, 11] and FLUKA [12, 13] predictions. A flowchart of the experiment is provided in Figure 2.

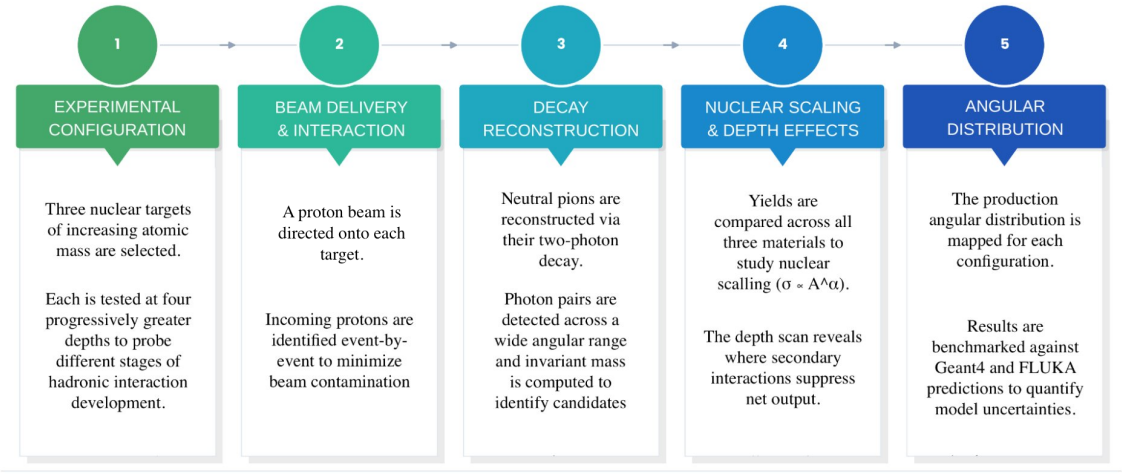

Figure 2: Flowchart of our experiment.

4 Simulation Studies

Simulations were performed using Geant4[10, 11], FLUKA[12, 13], and Flair [14] to validate the setup and guide the experimental design. Running both codes independently allows cross-checking of predictions and quantification of model-dependent uncertainty. Simulation outputs are available at:

Simulation Results: Google Drive

4.1 Geant4 Simulations

The 12 targets were placed in front of a 1 GeV/c proton beam. The `QGSP_BERT` physics list was used. From the resulting secondaries, the kinetic energies (T_{π^0}) and the angles made with the Z axis ($\theta_{\pi^0} = \cos^{-1}(\hat{p} \cdot \hat{z})$) of the π^0s were recorded at the point of production inside the target. A total of 10^6 protons were simulated. The results were saved in ROOT files [15] and plotted subsequently.

Geant4 predictions for all 12 configurations are shown in Table 2.

Setup n	π^0 Yield	$\langle T_{\pi^0} \rangle$ (MeV)	$\sigma(T_{\pi^0})$ (MeV)	$\langle \theta_{\pi^0} \rangle$ (rad)	$\sigma(\theta_{\pi^0})$ (rad)
1	12095	168.6	139.4	1.139	0.7129
2	34390	165.5	139.5	1.148	0.7159
3	54010	163.3	137.3	1.152	0.7169
4	71537	160.9	135.6	1.156	0.7185
5	12693	166.0	140.1	1.153	0.7119
6	35785	163.5	138.3	1.154	0.7152
7	56412	160.5	135.7	1.160	0.7182
8	74247	157.5	133.4	1.164	0.7175
9	17913	148.5	132.7	1.261	0.7238
10	48256	143.9	130.3	1.268	0.7302
11	72345	139.3	126.3	1.271	0.7313
12	90815	135.2	122.7	1.278	0.7297

Table 2: Geant4 simulation results for all 12 target configurations.

In the Geant4 figures, the X axes show energies in MeV and angles in radians, while the Y axes show the bin entries. Example plots from the results are shown in Figures 3 and 4.

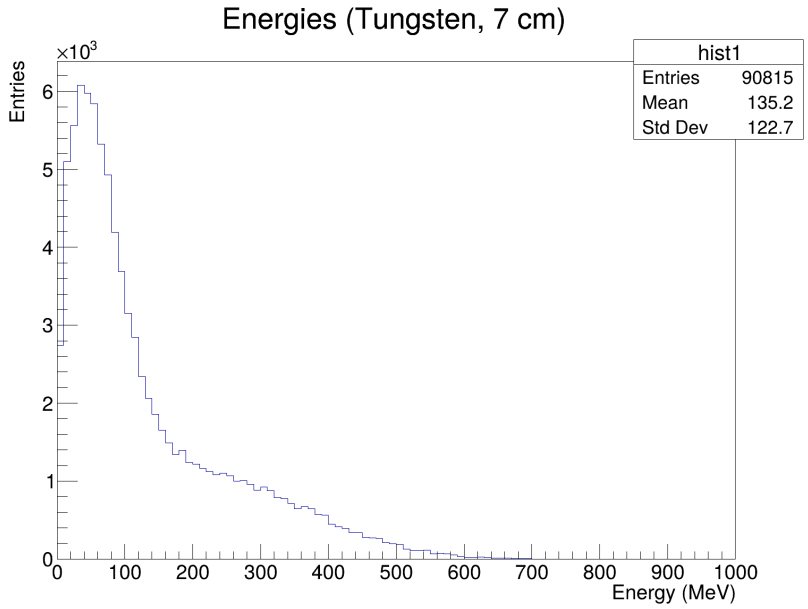

Figure 3: Geant4 simulation of π^0s kinetic energy distribution for a 7 cm tungsten target.

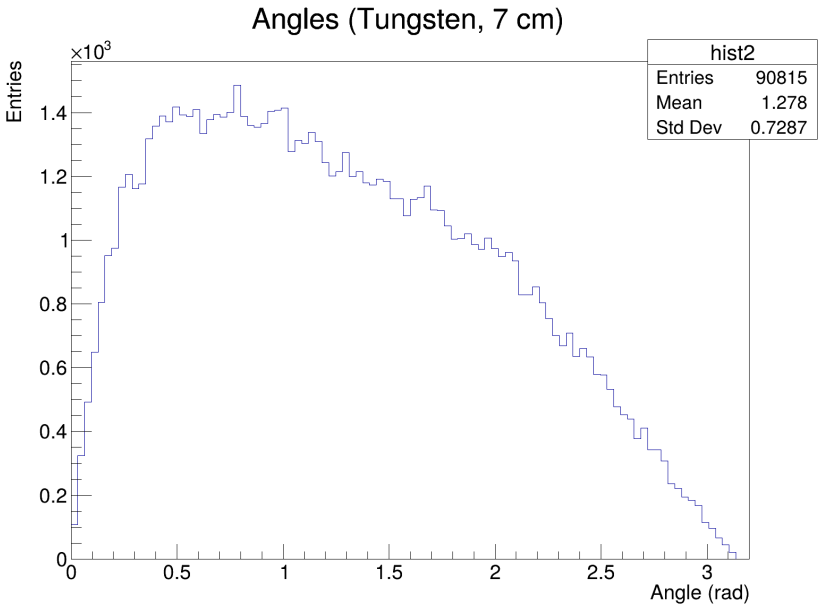

Figure 4: Geant4 simulation of π^0s angular distribution for a 7 cm tungsten target.

4.2 FLUKA Simulations

A 1 GeV/c proton beam was directed at 12 target configurations. The geometry and beam parameters were set using the Flair interface [14] with the `PRECISIO` card, which enables recommended physics settings for this energy range. A total of 10^6 protons were incident on the targets, and the resulting π^0 production was tracked. Kinetic energies (T_{π^0}) and Z-axis distributions ($\hat{p} \cdot \hat{z}$) were recorded using a user routine that scores secondary particles at their production point. The angles were calculated and the data were plotted using the Matplotlib library [16]. FLUKA results for all configurations are listed in Table 3.

Setup n	π^0 Yield	$\langle T_{\pi^0} \rangle$ (MeV)	$\sigma(T_{\pi^0})$ (MeV)	$\langle \theta_{\pi^0} \rangle$ (rad)	$\sigma(\theta_{\pi^0})$ (rad)
1	1160	80.72	79.60	1.4386	0.7316
2	3200	85.40	93.71	1.4684	0.7363
3	4577	81.37	83.99	1.4561	0.7347
4	5410	82.40	84.15	1.4604	0.7492
5	1292	71.87	72.30	1.4556	0.7323
6	3575	71.40	69.19	1.4328	0.7473
7	5012	73.88	74.52	1.4567	0.7466
8	5858	71.24	75.86	1.4687	0.7479
9	1859	20.11	30.37	1.5390	0.7326
10	4162	20.64	42.95	1.5458	0.7460
11	5220	20.03	36.42	1.5345	0.7494
12	5301	20.57	38.51	1.5299	0.7483

Table 3: FLUKA simulation results for all 12 target configurations.

In the FLUKA figures, the X axes show energies in GeV and angles in radians, while the Y axes show the bin entries. Example plots from the results are shown in Figures 5 and 6.

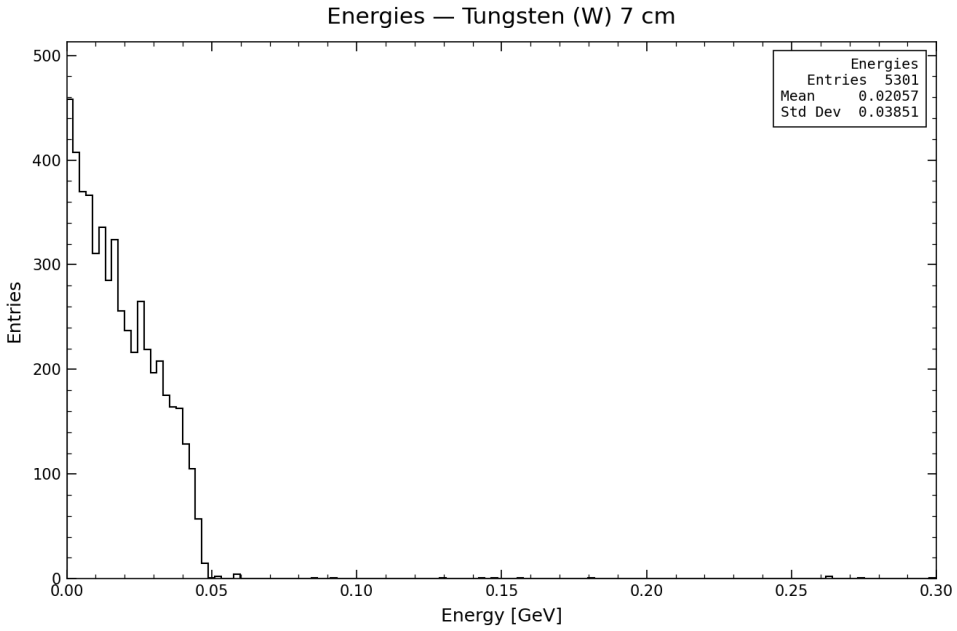

Figure 5: FLUKA simulation of π^0s kinetic energy distribution for a 7 cm tungsten target.

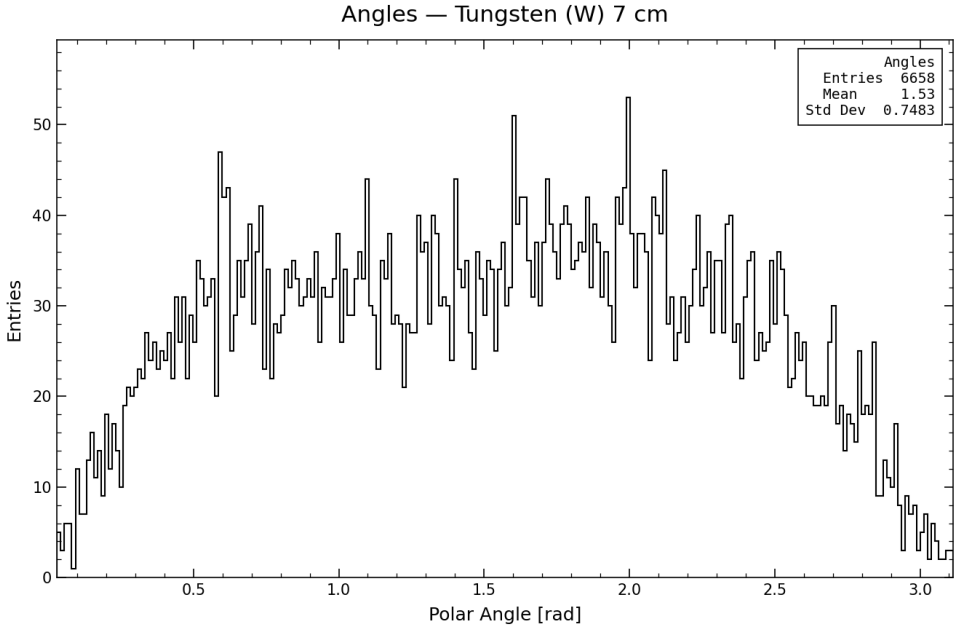

Figure 6: FLUKA simulation of π^0s angular distribution for a 7 cm tungsten target.

4.3 Comparison of Simulation Results

According to the Geant4 results, the π^0 yield and the angles of the π^0s increases while the kinetic energies of the π^0s decreases with the nuclear mass number and the target depth. There are fewer π^0s with higher energies and the angles of the π^0s have a larger spread.

According to the FLUKA results, the π^0 yield increases with the nuclear mass number and the target depth. The energies of the π^0s decreases and the their angles increases with the nuclear mass number, but there are no clear trends as the target depth changes. The energies are much more concentrated, but the angles spread further.

In both simulation groups, the trends as the nuclear mass number and the depth change seem to be similar. However, there are also clear differences in exact numbers. First, the ratio of Geant4's π^0 yield to the FLUKA's is around 10 for smaller depths, and increases to around 17 for 7 cm. The ratio of Geant4's mean energies of the π^0s to the FLUKA's is around 2 for iron and copper, but increases to 7 for tungsten. The energies of the π^0 are more spread out according to the Geant4 results, while the FLUKA results imply a sharp peak at low kinetic energies (20–85 MeV). Finally, there is around 0.3 radians of difference between the angles of the π^0s provided by Geant4 and FLUKA, but their spreads are similar. The differences are thought to be caused by the use of different physics models.

5 Machine Learning-Based Signal and Background Separation

As a future development, we plan to train a classifier to distinguish genuine $\pi^0 \to \gamma\gamma$ events from accidental coincidences and charged-particle leakage, using calorimeter energy depositions and timing as input features [17]. This would complement the cut-based analysis and improve the signal-to-noise ratio, especially at large angles where the background is highest. This is left as a follow-up study after the primary physics results are established.

6 Schedule

Day	Activity
Day 1	Setting up the detectors
Day 2	Setup 1
Day 3	Setup 2
Day 4	Setup 3
Day 5	Setup 4
Day 6	Setup 5 and data analysis of Iron (Fe)
Day 7	Setup 6
Day 8	Setup 7
Day 9	Setup 8
Day 10	Setup 9 and data analysis of Copper (Cu)
Day 11	Setup 10
Day 12	Setup 11
Day 13	Setup 12
Day 14	Data analysis of Tungsten (W) and Conclusions

Table 4: Planned schedule for the beamtime period.

7 Why We Want to Go

We are seven students from Istanbul united by a shared dream: to do real particle physics. Months of debugging code and arguing over simulation outputs brought us here, with

each member taking ownership of a different part (Geant4, FLUKA, detector layout, data analysis, outreach), and every section of this proposal genuinely understood by all.

We are thousands of kilometres from the nearest accelerator, in a country where most students never encounter a working detector. BL4S is the only programme that can place students like us at a real beamline, and we arrive ready, with a complete experimental design and fully validated simulations in two independent codes, to see what nature actually says. We hope to take away not just data, but the confidence that students from anywhere can contribute to frontier physics.

8 Outreach

We built *Pi Zero Academy*, an educational platform bringing particle physics to secondary school students through articles, animations, and podcasts. If selected, we will document the beamtime and publish the experience, including a team introduction video, as platform content for classrooms that have never visited CERN.
https://pizeroacademy.com/

Acknowledgements

We thank Merve Biçmen, Uğur Karataş and Nilay Bostan for useful discussions during the preparation of this work, and our school administration for providing computational resources.

References

[1] Workman, R. L., et al. (Particle Data Group). (2022). Review of Particle Physics. *Progress of Theoretical and Experimental Physics* **2022**, 083C01. https://doi.org/10.1093/ptep/ptac097

[2] Norbury, J. W., and Townsend, L. W. (2007). Parameterized total cross sections for pion production in nuclear collisions. *Nuclear Instruments and Methods in Physics Research Section B* **254**(2), 187–192. https://doi.org/10.1016/j.nimb.2006.11.054

[3] Abgrall, N., et al. (NA61/SHINE Collaboration). (2016). Measurements of $\pi^{\pm}$, $K^{\pm}$, K^0_S, Λ and proton production in proton–carbon interactions at 31 GeV/c with the NA61/SHINE spectrometer at the CERN SPS. *The European Physical Journal C* **76**(2), 84. https://doi.org/10.1140/epjc/s10052-016-3898-y

[4] Acharya, S., et al. (ALICE Collaboration). (2017). Production of π^0 and η mesons up to high transverse momentum in pp collisions at $\sqrt{s} = 2.76$ TeV. *The European Physical Journal C* **77**(5), 339. https://doi.org/10.1140/epjc/s10052-017-4890-x

[5] Coplowe, D., et al. (MINERvA Collaboration). (2020). Probing nuclear effects with neutrino-induced charged-current neutral pion production. *Physical Review D* **102**(7), 072007. https://doi.org/10.1103/PhysRevD.102.072007; Erratum: *Phys. Rev. D* **110**, 059903 (2024).

[6] Aphecetche, L., et al. (TAPS Collaboration). (2001). Hard photon and neutral pion production in cold nuclear matter. *Physics Letters B* **519**(1–2), 8–14. https://doi.org/10.1016/S0370-2693(01)01084-X

[7] CERN Beamline for Schools. (2026). Beams and Detectors: Beamline for Schools 2026. https://beamlineforschools.cern/wp-content/uploads/2026/02/Beams_Detectors_BL4S_2026.pdf Accessed: March 2026.

[8] Workman, R. L., et al. (Particle Data Group). (2022). Atomic and nuclear properties of materials. In *Review of Particle Physics*, *Progress of Theoretical and Experimental Physics* **2022**, 083C01, Section 6. https://doi.org/10.1093/ptep/ptac097; see also https://pdg.lbl.gov/2024/AtomicNuclearProperties/

[9] Cronin, J. W., Frisch, H. J., Shochet, M. J., Boymond, J. P., Mermod, R., Piroué, P. A., and Sumner, R. L. (1975). Production of hadrons at large transverse momentum at 200, 300, and 400 GeV. *Physical Review D* **11**(11), 3105–3123. https://doi.org/10.1103/PhysRevD.11.3105

[10] Agostinelli, S., et al. (Geant4 Collaboration). (2003). GEANT4: a simulation toolkit. *Nuclear Instruments and Methods in Physics Research Section A* **506**(3), 250–303. https://doi.org/10.1016/S0168-9002(03)01368-8

[11] Allison, J., et al. (Geant4 Collaboration). (2016). Recent developments in Geant4. *Nuclear Instruments and Methods in Physics Research Section A* **835**, 186–225. https://doi.org/10.1016/j.nima.2016.06.125

[12] Ahdida, C., et al. (2022). New Capabilities of the FLUKA Multi-Purpose Code. *Frontiers in Physics* **9**, 788253. https://doi.org/10.3389/fphy.2021.788253

[13] Battistoni, G., et al. (2015). Overview of the FLUKA code. *Annals of Nuclear Energy* **82**, 10–18. https://doi.org/10.1016/j.anucene.2014.11.007

[14] Donadon, A., Hugo, G., Theis, C., and Vlachoudis, V. (2024). FLAIR3 – recasting simulation experiences with the Advanced Interface for FLUKA and other Monte Carlo codes. *EPJ Web of Conferences* **302**, 11005. https://doi.org/10.1051/epjconf/202430211005

[15] Brun, R., and Rademakers, F. (1997). ROOT: An object oriented data analysis framework. *Nuclear Instruments and Methods in Physics Research Section A* **389**(1–2), 81–86. https://doi.org/10.1016/S0168-9002(97)00048-X

[16] Hunter, J. D. (2007). Matplotlib: A 2D graphics environment. *Computing in Science & Engineering* **9**(3), 90–95. https://doi.org/10.1109/MCSE.2007.55

[17] Bourilkov, D. (2019). Machine and Deep Learning Applications in Particle Physics. *International Journal of Modern Physics A* **34**(35), 1930019. https://doi.org/10.1142/S0217751X19300199